Chemical Modification of the Third Strand: Differential Effects on Purine and Pyrimidine Triple Helix Formation†

Martin Mills,‡ Paola B. Arimondo,‡ Laurent Lacroix,‡ Thérèse Garestier,‡ Horst Klump,§ and Jean-Louis Mergny*,‡

Laboratoire de Biophysique, Muséum National d'Histoire Naturelle, INSERM U 201, CNRS UMR 8646, Paris, France, and Department of Molecular & Cell Biology, University of Cape Town, Republic of South Africa

Received May 31, 2001

ABSTRACT: DNA triple helices offer exciting perspectives toward oligonucleotide-directed control of gene expression. Oligonucleotide analogues are routinely used with modifications in either the backbone or the bases to form more stable triple-helical structures or to prevent their degradation in cells. In this article, different chemical modifications are tested in a model system, which sets up a competition between the purine and pyrimidine motifs. For most modifications, the $\Delta H°$ of purine triplex formation is close to zero, implying a nearly temperature-independent affinity constant. In contrast, the pyrimidine triplex is strongly favored at lower temperatures. The stabilization induced by modifications previously known to be favorable to the pyrimidine motif was quantified. Interestingly, modifications favorable to the GT motif (propynyl-U and dU replacing T) were also discovered. In a system where two third strands compete for triplex formation, replacement of the GA or GT strand by a pyrimidine strand may be observed at neutral pH upon lowering the temperature. This purine-to-pyrimidine triplex conversion depends on the chemical nature of the triplex-forming strands and the stability of the corresponding triplexes.

Triple helices were first observed in 1957 for polyribonucleotides (*1*). This observation gave rise to a new approach for sequence-specific recognition of double-stranded DNA: an oligonucleotide can recognize a double-stranded DNA target in a sequence-specific manner and form a local triple helix (*2, 3*). Intermolecular triple helix formation has been conceived as a possible tool to control gene expression at the transcriptional level (*4*) or induce site-specific mutations (*5*). At least three structural classes of triple helix exist that differ in the base composition of the third strand, in the relative orientation of the phosphate−deoxyribose backbone, and in the thermodynamic parameters (*6*). In the first class, the pyrimidine motif (TC motif), the third strand binds parallel to the purine strand of the duplex by Hoogsteen hydrogen bonds, forming T·A*T and C·G*C+ triplets. This class of triple helix is stabilized by an acidic pH. In the second class, the GA motif, oligonucleotides containing guanines and adenines bind in an antiparallel orientation to the purine strand of the duplex by reverse-Hoogsteen hydrogen bonds, forming C·G*G and T·A*A base triplets. The third class of oligonucleotides composed of thymines and guanines, the GT motif, can bind either parallel or antiparallel to the purine strand of the duplex, depending on the base sequence (*7*). Some triple helices are hybrids between these different classes: a "GTA" triplex is formed when C·G*G, T·A*T, and T·A*A triplets are present in the same structure (*8*); a "TCG" triplex with a parallel orientation of the third strand is formed with Hoogsteen T·A*T, C·G*C+, and C·G*G base triplets (*9*). A high divalent cation concentration and a relatively high divalent/monovalent cation concentration ratio are often required for GT, GA, and GTA triple helix formation.

Several problems still limit the use of oligonucleotides as potential drugs such as cell penetration of the TFO[1] and accessibility of the DNA target. Chemically modified oligonucleotides have been designed to enhance their physiological stability and to overcome the rapid degradation of phosphodiester oligonucleotides by cellular nucleases. Different modifications have been proposed involving either the phosphate group [phosphorothioates (*10*), phosphorodithioates, methylphosphonates (*11*)] or the sugar−phosphate backbone [2′-*O*-methyl-nucleotides (*12, 13*), phosphoramidates (*14*), morpholino (*15*), and PNA (*16*)]. Binding of a third-strand oligonucleotide to a target duplex generally results in a thermodynamically weaker interaction than observed for duplex formation itself (*6, 17, 18*). Base modifications have therefore been studied in an attempt to stabilize triple-stranded structures [e.g., 5-methyl-dC (*19*) and 5-propynyl-dU (*20*) for C and T, respectively].

In this report, we address the possibility of forming a triple helix with various modified TFOs compared to isosequential phosphodiester oligonucleotides (Figure 1A,B). We limited our analysis to commercially available oligonucleotides. We used a model system, which allows the formation of 9 base

† This work was supported in part by CNRS, INSERM, and French−South African CNRS/FRD (98N2/0851) and Ministère de la Recherche/FRD grants.

* To whom correspondence should be addressed at the Laboratoire de Biophysique, 43 rue Cuvier, 75231 Paris cedex 05, France. Fax: (33-1) 40 79 37 05, E-mail: mergny@vnumail.com.

‡ Muséum National d'Histoire Naturelle, INSERM U 201.

§ University of Cape Town.

[1] Abbreviations: EMSA, electrophoretic mobility shift assay; FRET, fluorescence resonance energy transfer; Py, pyrimidine; Pu, purine; TFO, triplex-forming oligonucleotide; UV, ultraviolet; mP, methylphosphonate; PS, phosphorothioate; mC, 5-methylcytosine; bU, 5-bromouracil; dU, deoxyuracil; pU, 5-propynyluracil; T_m, temperature of half-dissociation.

10.1021/bi011122m CCC: $22.00
Published on Web 12/08/2001

Table 1: List of the Oligonucleotides Tested in This Study[a]

name	sequence (5′→3′)	backbone	sugar (2′)	ϵ ($\times 10^{-3}$)
	Duplex Short Strands			
9Pu	GAAGAGAGG	−	H	104
9Py	CCTCTCTTC	−	H	69
	Pyrimidine Motif Clamp			
22Py	CCTCTCTTC**CCTT***CTTCTCTCC*	−	H	168
22PyS	CCTCTCTTC**CCTT***CTTCTCTCC*	PS	H	168
22PymP	CCTCTCTTC**CCTT***CTTCTCTCC*	mP	H	168
22PyRNA	CCTCTCTTC**CCTT***cuucucucc*	−	OH	172
22PyOMe	CCTCTCTTC**CCTT***cuucucucc*	−	OMe	172
22PymC	CCTCTCTTC**CCTT***MTTMTMTMC*	−	H	168
22PydU	CCTCTCTTC**CCTT***CUUCUCUCC*	−	H	172
22PypU	CCTCTCTTC**CCTT***CPPCTCPCC*	−	H	171
22PypUmC	CCTCTCTTC**CCTT***MPPMPMPMC*	−	H	172
22PyOmC	CCTCTCTTC**CCTT***muumumumc*	−	OMe	172
	(G, T) Motif Clamp			
22GT	GAAGAGAGG**CCTT***GGTGTGTTG*	−	H	218
22GTS	GAAGAGAGG**CCTT***GGTGTGTTG*	PS	H	218
22GTmP	GAAGAGAGG**CCTT***GGTGTGTTG*	mP	H	215
22GTRNA	GAAGAGAGG**CCTT***ggugugugug*	−	OH	222
22GTOMe	GAAGAGAGG**CCTT***ggugugugug*	−	OMe	222
22GdU	GAAGAGAGG**CCTT***GGUGUGUUG*	−	H	222
22GbU	GAAGAGAGG**CCTT***GGBGBGBBG*	−	H	222
22GpU	GAAGAGAGG**CCTT***GGPGPGPPG*	−	H	222
	(G, A) Motif Clamp			
22GA	GAAGAGAGG**CCTT***GGAGAGAAG*	−	H	235
22GAS	GAAGAGAGG**CCTT***GGAGAGAAG*	PS	H	235
22GAmP	GAAGAGAGG**CCTT***GGAGAGAAG*	mP	H	235
22GARNA	GAAGAGAGG**CCTT***ggagagaag*	−	OH	235

[a] Column 1 lists the abbreviated name, followed by the primary sequence of the oligonucleotide (column 2), and the extinction coefficient at 260 nm calculated according to Cantor et al. (far-right column) (*25*). The abbreviated name follows the following convention: the length of the oligomer (in nucleotides) is followed by the nature of the strand involved in the Watson−Crick duplex (for short oligonucleotides) or the nature of the third strand (Py, GA, or GT). The sequence is written 5′ to 3′ for all oligonucleotides. For the 22-mers, the primary sequences have been designed with the following rules: the Watson−Crick complementary bases are located at the start of the sequence (5′). They are followed by the same connecting loop (CCTT, boldface characters) and then by the triplex part (italics). RNA and 2′-OMe bases are shown by lowercase letters. Abbreviations: M = 5-methylcytosine; P = 5-propynyluracil (or "pU"); B = 5-bromouracil (or "bU"). ϵ is given in M^{-1} cm^{-1}.

triplets [T·A*T and C·G*C+ in the pyrimidine (TC) motif, T·A*A and C·G*G in the purine (GA) motif, T·A*T and C·G*G in the GT motif (*6*, *8*)] on an oligopurine−oligopyrimidine target duplex of 9 base pairs. The sequences of all oligonucleotides are given in Table 1. The asymmetry of the sequence is a design feature which allows a core Watson−Crick duplex to form in all cases without interference from the additional third strand. UV melting was used to monitor the stability of the various complexes, and, based on the T_ms, phase diagrams were constructed indicating the relative stabilities of the complexes. Only a few articles deal with a comparison of all three types of oligodeoxynucleotide third strands (*6*, *21*−*24*), and none deal with a quantitative comparison of commercially available chemical modifications of a TFO in the three motifs.

EXPERIMENTAL PROCEDURES

Oligonucleotides. Oligodeoxynucleotide probes were synthesized by Eurogentec (Belgium) or Genosys (U.K.) on the 0.2 μmol scale. Purity was checked by gel electrophoresis. All concentrations were expressed in strand molarity using a nearest-neighbor approximation for the absorption coefficients of the unfolded species (*25*).

Nomenclature and Design of the System. TC, GT, and GA triplexes refer to the nature of the bases present in the third strand involved in Hoogsteen or reverse-Hoogsteen hydrogen bonding. Concerning the base triplets, as an example, a C·G*G triplet is obtained when base G in a third strand recognizes the Watson−Crick C·G base pair and forms specific hydrogen bonds, "*", with the guanine on the purine-rich strand of the duplex. The sequences of most of the oligodeoxynucleotides investigated are listed in Table 1. We adopted the following convention for all the oligodeoxynucleotides: the first number indicates the length of the oligodeoxynucleotide followed by the composition of the third strand (Py or GT/GA) followed by the modification (e.g., S for a phosphorothioate backbone and dU for deoxyuracil base substitution). The simple Pu/Py label indicates whether the oligonucleotide is involved in the purine or pyrimidine part of the duplex. Most melting curves shown in this study were perfectly reversible, and no hysteresis was obtained [i.e., the melting profiles obtained when heating or cooling the sample were superimposable, in contrast to what is observed for intermolecular triplexes (*26*)]. The hairpin plus single-strand system allowed relatively short strands to be used to form a triplex which is distinguishable from the duplex by UV melting experiments.

UV Absorption Studies. All experiments were performed, unless otherwise specified, in a 10 mM cacodylate buffer containing 0.1 M LiCl and variable concentrations of $MgCl_2$ (0−20 mM), at 1−20 μM oligonucleotide strand concentration. Thermal denaturation profiles were obtained with a Kontron Uvikon 940 spectrophotometer as previously described (*6*). Absorbance measurements were performed at each temperature interval at 245, 260, 295, and 405 nm (the control wavelength).

Extraction of the Thermodynamic Parameters. The quality of most melting curves allowed a thermodynamic analysis of the transition using a previously described model (*6*). Although these thermodynamic parameters were obtained through model-dependent determinations, we believe, based on previous observations (*6*), that our measurements accurately reflect the $\Delta H°$ and $\Delta S°$ of duplex and triplex formation.

Electrophoretic Mobility Shift Assay (EMSA). Either duplex strand was ^{32}P-end-labeled with T4 polynucleotide kinase and [γ-^{32}P]ATP, according to the manufacturer's protocol. The binding reaction was performed overnight at 37, 20, or 4 °C in 20 μL of 50 mM Hepes, pH 7.2, 0.1 M LiCl, 10 mM $MgCl_2$, 10% sucrose, and 0.5 μg/μL tRNA carrier. The solution contained 0.1 pmol of the end-labeled probe (20 000−40 000 cpm). The binding mixtures were electrophoresed at 4 °C for 3 h (10 V/cm) on a 15% nondenaturing polyacrylamide (bis/acryl 19:1), 50 mM Hepes, pH 7.2, 10 mM $MgCl_2$ gel, dried, and analyzed with an SP phosphorimager (Molecular Dynamics). The apparent K_d is defined as the TFO concentration required to shift 50% of the duplex radioactivity in the retarded band (triplex).

RESULTS

The triplex system is shown in Figure 1C. The sequence was arranged to be asymmetric to allow for a unique orientation of the third strand: the loop directs the "third strand" to an antiparallel orientation (for GA, GT, and GTA third strands) or a parallel orientation (for a CT third strand) with respect to the purine strand of the duplex (*6*). The asymmetry of the sequence also allows a core Watson−Crick duplex to form in all cases without interference from the additional third strand. The stabilities of these complexes were compared with the stability of the short Watson−Crick duplex, formed with two short strands of identical length. Another consequence of this covalent link of the third strand with one strand of the duplex is to increase the stability of the triplex and to speed up the kinetics of triplex formation as a result of the intramolecular nature of the reaction once the duplex is formed.

Stability of the Pyrimidine Triplex. The melting of the duplex (9Py/9Pu) is monophasic, concentration-dependent, and pH-independent in the pH range 5−7.8 (*6*). The melting of the unmodified pyrimidine triplex (22Py/9Pu) is biphasic at pH 6.8 or higher (Figure 2C) and monophasic below this pH [Figure 2A,B, open squares, and ref (*6*)]. At pH ≥7.1, the two transitions are reasonably resolved: the first low-temperature transition is assigned to the conversion of a triplex to a duplex-plus-tail species and the second transition, at higher temperature, to the melting of the duplex into single strands (*6*). From the scheme presented in Figure 1C, one can see that the first transition should correspond to an intramolecular rearrangement, whereas the second transition involves the separation of two strands. The T_m of the first transition was concentration-independent, as expected for an intramolecular reaction, whereas the T_m of the second transition increased when higher strand concentrations were used (*6*). At pH 6.0, direct melting of the triplex into single strands is observed, leading to a significant hyperchromism at 260 nm (Figure 2A) and hypochromism at 295 nm (Figure 2B), as previously described for DNA structures involving

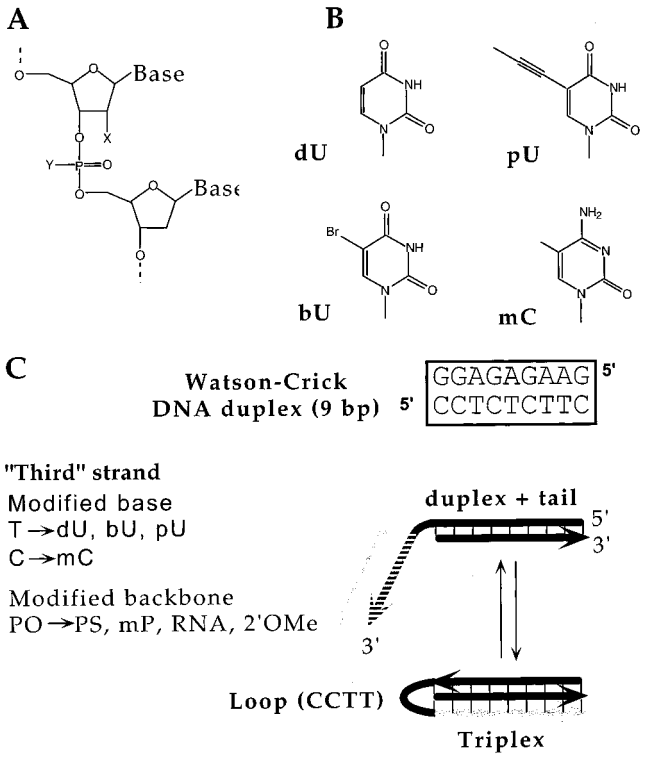

FIGURE 1: Presentation of the system. (A) Backbone modifications used in this study. PO: X═H, Y═O− (DNA); X═OH, Y═O− (RNA); X═OCH_3, Y═O− (2′-OMe). PS: X═H, Y═S− (phosphorothioate). mP: X═H, Y═CH_3 (methylphosphonate). (B) Base modifications used in this study. dU, uracil ("U" in Table 1); mC, 5-methylcytosine ("M" in Table 1); pU, 5-(1-propynyl)uracil ("P" in Table 1); bU, 5-bromouracil ("B" in Table 1). (C) Possible complexes resulting from the association of two strands. One long strand may associate with a short strand to form a duplex + overhanging single strand or a triplex. The sequence and orientation of the 9 bp duplex are given. Only the triplex part of the oligonucleotide (hatched) is chemically modified: the Watson−Crick strands and the 4-base loop are composed of regular DNA.

cytosine protonation (*27*, *28*). This variation at 295 nm is the result of the difference in absorption (ϵ) between cytosine and N3-protonated cytosine (*29*). The melting temperature of the triplex was pH-dependent (Figure 3, squares).

At higher pHs, two transitions are usually obtained (Figure 2C) corresponding to the unfolding of the third strand (triplex-to-duplex) and the dissociation of the duplex into single strands. A plot of T_m vs pH produces a phase diagram which helps to assign the various species formed (Figure 3). The impact of the third-strand modifications is immediately apparent in the shifting of the triplex-to-coil (III to I) and triplex-to-duplex (III to II) phase boundaries. As expected, the phase boundary of the duplex-to-coil (II to I) transition remains relatively unaffected by the third-strand modifications. The TC triplex melts to a duplex-plus-tail with a T_m of 24.5 °C at pH 6.9 (10 mM sodium cacodylate, 0.1 M LiCl, 10 mM $MgCl_2$) and melts from triplex to random coil with a T_m of 40 °C at pH 6. On substitution of the phosphate backbone with phosphorothioates, the T_m drops by 7.5 °C at pH 6 (Figure 2A, triangles, and Figure 3B for the phase diagram). A destabilization is also observed with the methylphosphonate substitution which lowers the T_m by 15.5 °C at pH 6 and the melting curve becomes biphasic (phase diagram: Figure 3C). The RNA and 2′-OMe analogues, however, are more stable and raise the T_m of both

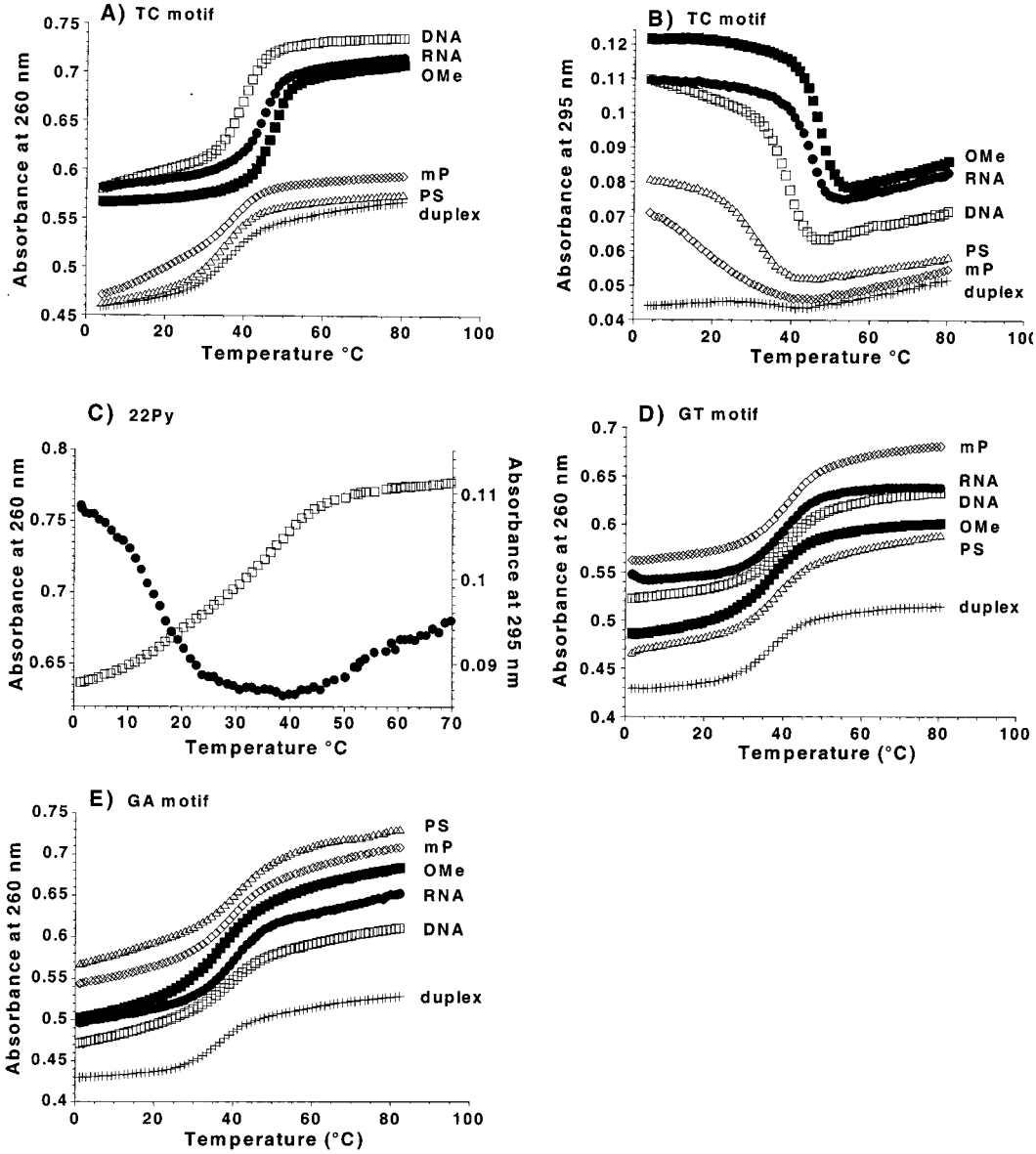

FIGURE 2: Denaturation profiles obtained for the different triplexes. (A) Pyrimidine triplexes with modified backbones (260 nm) at pH 6.0. (B) Pyrimidine triplexes with modified backbones (295 nm) at pH 6.0 (note the difference in the scale of the *y*-axis). (C) Unmodified pyrimidine triplex shown at two wavelengths (260 nm, open squares, left *y*-axis; and 295 nm, filled circles, right *y*-axis) at pH 7.1. (D) GT triplexes with modified backbones (260 nm) at pH 6.9. (E) GA triplexes with modified backbones (260 nm) at pH 6.9. In panels A−B and D−E, the melting profile of the duplex is shown for comparison (crosses). The melting profile of the reference, unmodified triplex (TC, GT, or GA) is depicted by open squares. RNA third strand, filled circles; 2′-OMe, filled squares; methylphosphonates ("mP"), diamonds; phosphorothioates ("PS"), triangles. Except in panel C, most triplex mixtures give only one transition, corresponding to the direct dissociation of triplexes into single strands. All experiments were performed in a 10 mM sodium cacodylate, 100 mM LiCl, 10 mM $MgCl_2$ buffer at the indicated pH. Strand concentration: 3 μM.

the triplex-to-coil transition by 5 and 7 °C, respectively, at pH 6 and the triplex-to-duplex transition by 11 and 12.5 °C, respectively, at pH 6.9 (phase diagram for 22PyOMe: Figure 3D). The base substitutions of propynyl-U for T and methyl-C for C raise the T_m of both the triplex-to-coil transition by 7.5 and 5.5 °C (pH 6), respectively, and the triplex-to-duplex transition (pH 6.9) by 12 and 10.5 °C, respectively. The phase diagrams for 22PymC and 22PypU are shown in Figure 3E and 3F, respectively. In constrast, the base substitutions of dU for T have little effect on the triplex-to-coil transition and a small destabilizing effect on the triplex-to-duplex transition (not shown). The double modification of the phosphate backbone for 2′-OMe and base C for mC raises the T_m of the triplex-to-coil transition by 10.5 °C (pH 6) and that of the triplex-to-duplex transition by 13.5 °C (pH 6.9). The second double modification of T for pU and C for mC raises the T_m of the triplex-to-coil transition (pH 6) by 15.5 °C and the triplex-to-duplex transition by 19.5 °C at pH 6.9. This double modification produces a pyrimidine motif triplex which is stable at room temperature and neutral pH with a T_m of 44 °C. As the stability of the triplex is increased (i.e., when a favorable modification is tested), the area corresponding to the region of triplex stability extends to the detriment of the duplex region (compare Figure 3H to Figure 3A). In constrast, a drop in triplex stability shrinks the region of triplex predominance in a phase diagram (Figure 3B,C).

The melting profiles were treated according to the method described previously (*6*). Most melting profiles gave reasonable linear fits for the monophasic triplex-to-coil transition

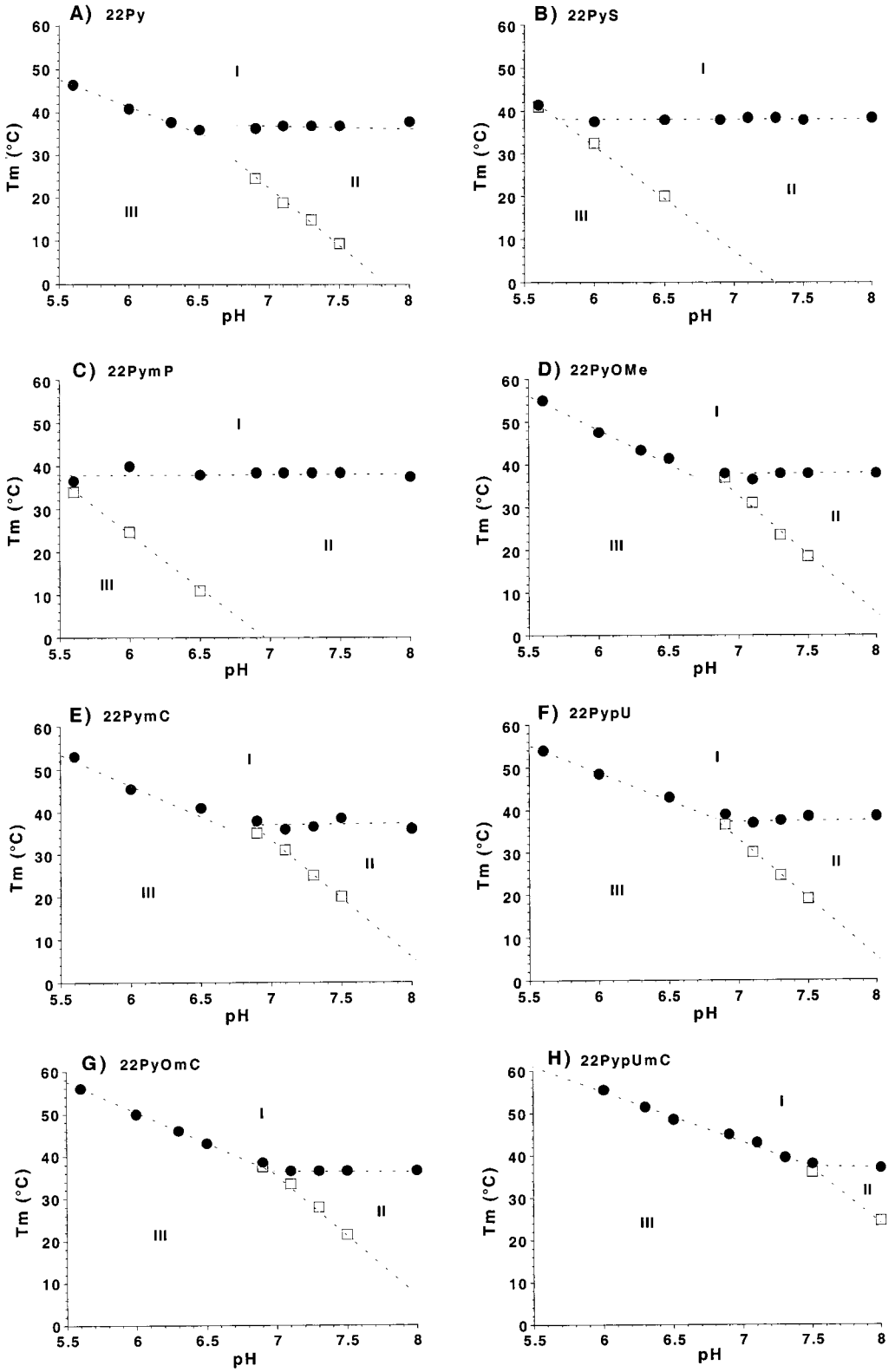

FIGURE 3: Phase diagrams for the pyrimidine triplexes. (A) 22Py, (B) 22PyS, (C) 22PymP, (D) 22PyOMe, (E) 22PymC, (F) 22PypU, (G) 22PyOmC, (H) 22PypUmC. All experiments were performed in 10 mM sodium cacodylate or acetate, 100 mM LiCl, 10 mM $MgCl_2$ buffer at variable pH with 3 μM strand concentration; the diagram is divided into three areas, labeled "I", "II", and "III", which correspond to melted strands, duplex + tail, and triplex species, respectively. The experimental midpoint of the triplex-to-duplex transition (determined at 295 nm) is indicated by open squares. The experimental position of the triplex or duplex to single strands (determined at 260 nm) is indicated by filled circles.

observed at pH 6.0 (not shown). This allowed us to estimate $-\Delta H°/R$ from the slope of the curve and $\Delta S°/R$ from the *y*-intercept (*6*). The numerical results for all oligonucleotides are summarized in Table 2. The $\Delta H°$ of formation of the 22Pytriplex from single strands is −118 kcal/mol, and subtracting the value of −67 kcal/mol ($\Delta H°$ of duplex formation) yields a $\Delta H°$ for third-strand association of −51 kcal/mol. Substituting T with dU and pU yields $\Delta H°$ values

Table 2: Thermodynamic Parameters Obtained for the Pyrimidine Motif Triplex[a]

oligos + 9Pu	T_m (°C)	$\Delta H°$ (kcal/mol)	$\Delta S°$ (cal mol^{-1} K^{-1})	$\Delta G°$ (40 °C) (kcal/mol)	K_d (40 °C) (M)
9Py	37	−67	−191	−7.6	4.8×10^{-6}
22Py	40	−118	−348	−8.6	9.5×10^{-7}
		Modified Backbone			
22PyS	32.5,[b] 37	*c*	*c*	*c*	
22PymP	27.5,[b] 38	*c*	*c*	*c*	
22PyRNA	45.5	−94	−269	−9.6	1.9×10^{-7}
22PyOMe	47.5	−121	−352	−11.0	1.9×10^{-8}
		Modified Bases			
22PydU	41	−114	−337	−8.6	9.5×10^{-7}
22PypU	48.5	−123	−357	−11.5	8.8×10^{-9}
22PymC	45.5	−163	−485	−11.2	1.4×10^{-8}
		Double Modification			
22PyOmC	50.5	−109	−311	−11.6	7.5×10^{-9}
22PypUmC	56	−135	−386	−14.6	5.9×10^{-11}

[a] The oligo mentioned in the first column is mixed with the 9Pu oligodeoxynucleotide. Buffer conditions are 10 mM sodium cacodylate in 0.1 M lithium chloride and 10 mM magnesium chloride at pH 6.0. [b] Determined at 295 nm (two transitions are observed as the triplex is destabilized and its melting is uncoupled from the duplex melting). [c] T_m1 corresponds to the triplex−duplex transition (for all other transitions, a direct melting of the triplex into single strands is observed at this pH; see Figure 2A).

Table 3: Thermodynamic Parameters Obtained for the GT Motif Triplex

complex + 9Py	T_m[a] (°C)	$\Delta H°$ (kcal/mol)	$\Delta S°$ (cal mol^{-1} K^{-1})	$\Delta G°$ (40 °C) (kcal/mol)	K_d (40 °C) (M)	relative stability[b]
9Pu	37.5	−64	−180	−7.8	4.4×10^{-6}	0.4
22GT	42	−73	−204	−9.0	7.9×10^{-7}	1
			Modified Backbone			
22GTS	40	−70	−197	−8.5	1.4×10^{-6}	0.6
22GTmP	42	−69	−191	−9.2	5.9×10^{-7}	1.3
22GTRNA	40	−78	−222	−8.5	1.5×10^{-6}	0.5
22GTOMe	39.5	−59	−163	−8.4	1.5×10^{-6}	0.5
			Modified Bases			
22GpU	43	−72	−200	−9.4	4.5×10^{-7}	1.8
22GbU	42.5	−66	−182	−8.8	8.4×10^{-7}	1
22GdU	44.5	−76	−212	−9.6	3.0×10^{-7}	2.7

[a] The T_m corresponds to the melting temperature of the duplex-to-coil or GT triplex-to-coil transition in 10 mM sodium cacodylate in 0.1 M LiCl and 10 mM $MgCl_2$ at pH 6.9. [b] Relative stability is deduced from K_d(GT)/K_d at 40 °C.

for third-strand formation of −47 and −56 kcal/mol, respectively. The double substitution of T with pU and of C with mC gives −68 kcal/mol.

Stability of the GT Triplexes. The melting behaviors of the GT triplexes were different: under all conditions tested, the transitions were monophasic (*6*), in agreement with the related system of Vo et al. (*30*). These transitions are very similar in shape as well as in hyperchromicity, which is identical to what is observed during the melting of the duplex, but they are shifted to higher temperatures (Figure 2D). These transitions could be analyzed as two-state bimolecular processes. The values of $\Delta H°$ given in Table 3 correspond to the formation of a triplex from single strands: they do not give a proper estimate of $\Delta H°$ of triplex formation when a third strand is added to a duplex. An uncoupling between the melting of a double and a triple helix was not observed for the GT (and GA; see next paragraph) triplexes, which never gave rise to two independent melting transitions. An indirect method was therefore used (*6*) to estimate the $\Delta H°$ of third-strand binding to a duplex taking advantage of the fact that thermodynamic values are state functions and independent of the reaction path. The $\Delta H°$ of third-strand binding is calculated as −9 kcal/mol for the GT third strand, and replacing T with dU gives −12 kcal/mol. The apparent K_d was calculated from the free energy and expressed as relative stability compared to the GT triplex. The duplex and GT triplex have a K_d of 4.4×10^{-6} and 7.9×10^{-7} M, respectively, at 40 °C (10 mM sodium cacodylate, 0.1 M LiCl, 10 mM $MgCl_2$, pH 6.9). Among the base substitutions, the GbU analogue is just as stable as the GT triplex, and the GpU and GdU analogues are 1.8 and 2.7 times more stable, respectively.

The effects of backbone and base modifications are displayed as plots of T_m as a function of magnesium ion concentration (Figure 4A,B). The methylphosphonate and phophorothioate analogues have similar T_ms and magnesium dependency as the phosphate GT triplex. The RNA and 2′-OMe analogues show slight magnesium dependency but are not significantly more stable than the duplex. As increasing [Mg^{2+}] leads to an increase in T_m, one may conclude that there is a net magnesium uptake upon triplex formation. This increase is also more pronounced for triplexes than for duplexes. For the GT and GdU triplexes at 40 °C, a net magnesium uptake of 0.92 and 1.47 ions/triplex was calculated, as compared to 0.38 for the duplex. The GpU and GdU analogues are more stable than the GT triplex, with the dU for T replacement being the most stabilizing.

To establish whether the mP backbone and the pU and dU for T base substitutions could stabilize an intermolecular triplex, we performed bandshift assays on a different system in which a 13 (d-GGTGGTGGTGGTG) or 15 (d-GGTG-GTGGTGGTGTT) base long oligonucleotide could bind to a 29 base pair DNA duplex (which includes the oligopyrimidine−oligopurine target sequence, Figure 5) (*31*). The affinity of the third strand for the duplex was tested by EMSA experiments at 4 °C in a 0.1 M LiCl, 10 mM $MgCl_2$, pH 7.2, 50 mM Hepes buffer with a radiolabeled duplex and increasing concentrations of the third strand. Although bandshift techniques tend to underestimate binding affinities (*32*), the apparent K_ds determined at 4 °C were ranked in agreement with the spectroscopic results with the exception of GTmP which is less stable than GT in the intermolecular system. The apparent K_ds rank as follows: 13GdU = 13GpU (0.4 μM) < 13GT (1 μM) < 13GTmp (2 μM); and 15GdU (0.5 μM) < 15GpU (0.9 μM) < 15GT (10 μM) < 15GTmP (15 μM).

Stability of the GA Triplexes. The melting behavior of the GA triplexes is reminiscent of the GT triplex (Figure 2E), and the unmodified GT and GA third strands were of similar affinity under all conditions judging from their melting temperatures (39.5 and 40 °C).

These transitions could be analyzed as two-state bimolecular processes. The values of $\Delta H°$ given in Table 4 correspond to the formation of a triplex from randomly coiled single strands: they do not give a proper estimate of $\Delta H°$ of triplex formation when a third strand is added to a duplex. Again, an uncoupling between the melting of a double and a triple helix was not observed for the GA triplexes, which never gave rise to two independent melting transitions. In

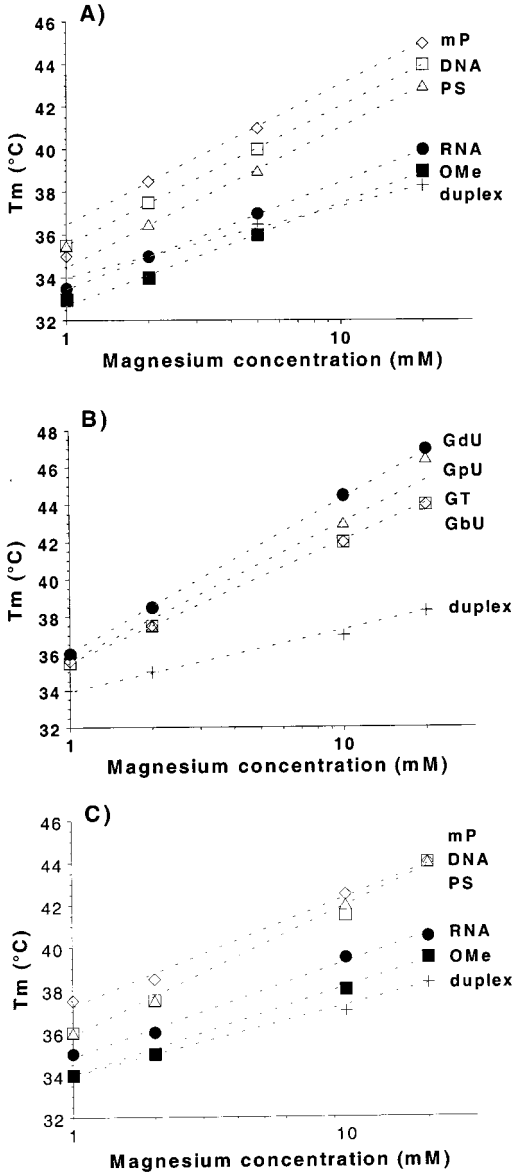

FIGURE 4: Magnesium concentration dependency of the GT and GA triplexes. (A) GT triplex: Effect of backbone modification (*x*-axis: log scale). (B) GT triplex: Effect of base modification (*x*-axis: log scale). (C) GA triplex: Effect of backbone modification (*x*-axis: log scale). The unmodified GT, GA triplexes and duplexes are shown in each curve by open squares and crosses, respectively. Experimental conditions: 10 mM sodium cacodylate buffer, 0.1 M LiCl, 1−20 mM $MgCl_2$ at pH 6.0.

terms of K_d, the GAS and GAmP analogues are 1.4 and 1.2 times as stable as the GA triplex whereas GARNA and GAOMe are destabilized.

The GA analogues (Figure 4C) show a similar trend of magnesium dependency to the GT analogues. The phosphate, phosphorothioate, and methylphosphonate GA triplexes have similar T_ms, while the RNA and 2′-OMe analogues are significantly less stable than the unmodified GA DNA triplex. The T_m difference with the duplex is hardly significant especially at low magnesium concentration, demonstrating that these triplexes are either not formed or very unstable.

Strand Exchange: GT vs TC Triplexes. It is possible to create a competition between the CT and GT third strands for the same duplex by combining two 22-base strands (Figure 6A). A triplex-to-triplex transition was reported

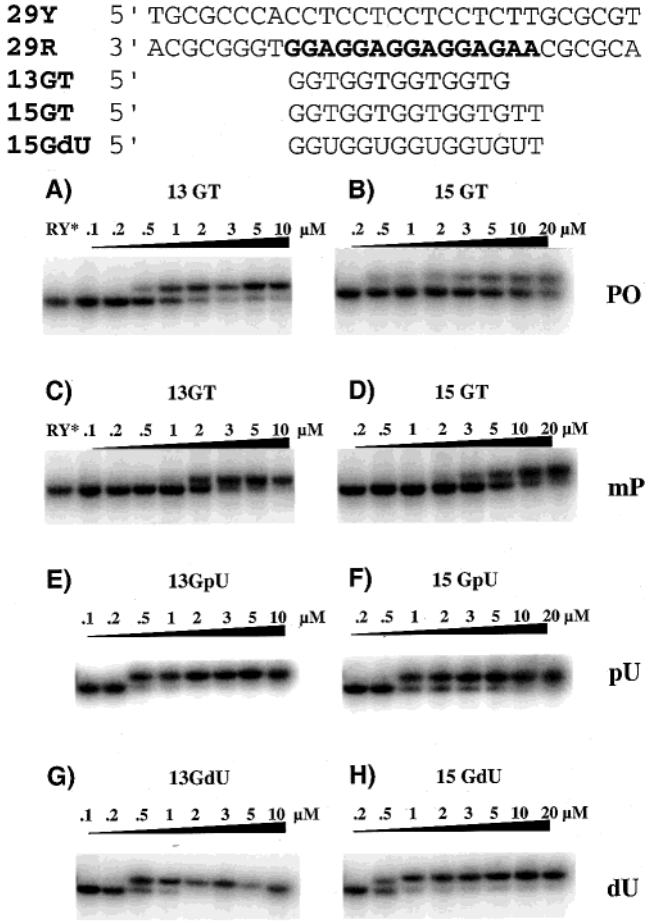

FIGURE 5: EMSA in the GT motif. Top: Sequence of the duplex and of the TFOs. (A) 13-mer, unmodified ("PO") TFO. (B) 15-mer, unmodified ("PO") TFO. (C) 13-mer, methylphosphonate ("mP") TFO. (D) 15-mer, methylphosphonate ("mP") TFO. (E) 13-mer, propynyl-dU ("pU") TFO. (F) 15-mer, propynyl-dU ("pU") TFO. (G) 13-mer, deoxyuracil ("dU") TFO. (H) 15-mer, deoxyuracil ("dU") TFO. The sequences of the radiolabeled duplex sequence and of the unmodified TFOs (13GT and 15 GT) are shown at the top. The TFO strand concentration (0.1−20 μM) is indicated above each lane. "RY*" corresponds to the duplex (no TFO added).

Table 4: Thermodynamic Parameters Obtained for the GA Motif Triplex

complex + 9Py	T_m[a] (°C)	$\Delta H°$ (kcal/mol)	$\Delta S°$ (cal mol^{-1} K^{-1})	$\Delta G°$ (40 °C) (kcal/mol)	K_d (40 °C) (M)	relative stability[b]
9Pu	37.5	−66	−188	−7.6	4.4×10^{-6}	0.4
22GA	41.5	−67	−189	−8.3	1.7×10^{-6}	1
22GAS	41.5	−64	−176	−8.4	1.3×10^{-6}	1.4
22GAmP	42	−63	−173	−8.5	1.4×10^{-6}	1.2
22GARNA	41	−61	−167	−8.4	2.7×10^{-6}	0.6
22GAOMe	39	−58	−160	−8.0	2.8×10^{-6}	0.6

[a] The T_m corresponds to the melting temperature of the duplex-to-coil or GA triplex-to-coil transition in 10 mM sodium cacodylate in 0.1 M LiCl and 10 mM $MgCl_2$ at pH 6.9. [b] Relative stability is deduced from K_d(GA)/K_d at 40 °C.

previously with unmodified oligodeoxynucleotides (*6*). A similar phenomenon occurred when modified TFOs were used. A significant hyperchromism at 295 nm is observed for TC, but not for GT or GA, triplex formation. Pyrimidine triplex formation involves cytosine protonation, and this hyperchromism is the result of the difference in absorption (ϵ) between cytosine and N3-protonated cytosine. Therefore, at this wavelength we can follow the T ↔ Ds or T ↔ T

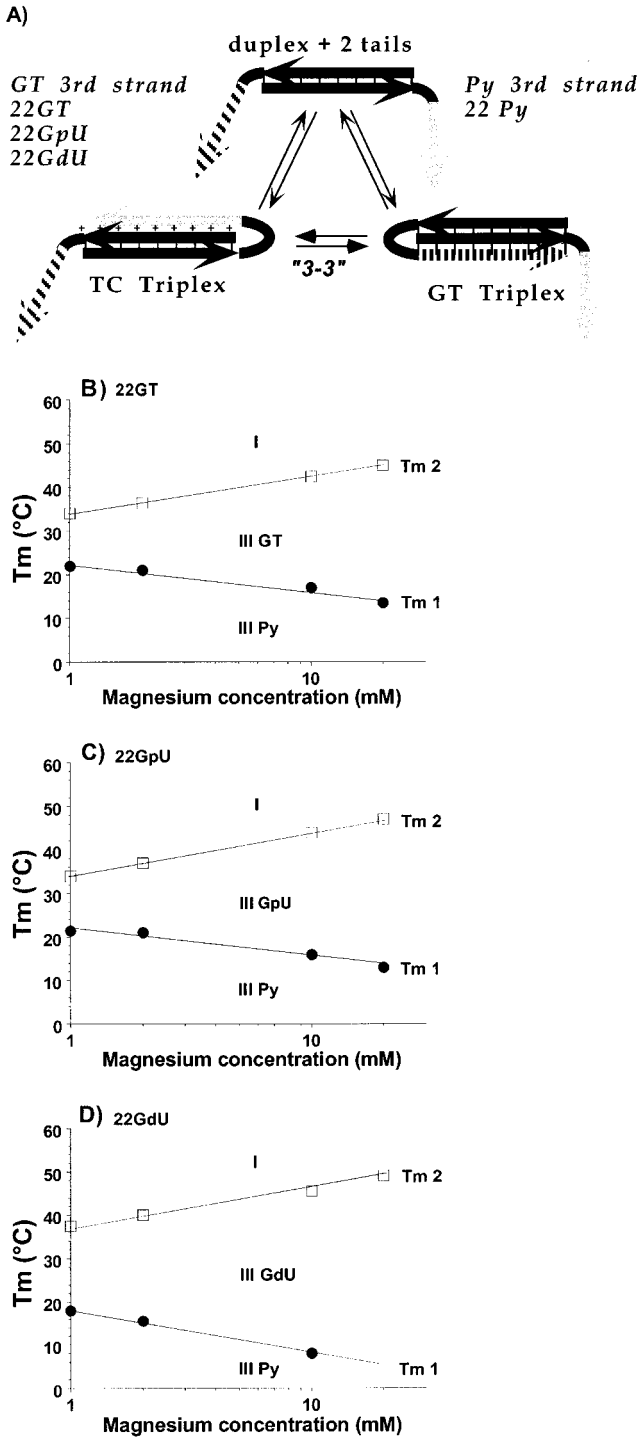

FIGURE 6: Phase diagram for the triplex-to-triplex transitions. (A) Scheme of the triplexes. The association of two long strands (22-mers) may lead to the formation of a duplex + 2 tails, or a TC triplex with an overhanging GT strand, or a GT triplex with an overhanging TC strand. (B) Phase diagram for the 22Py/22GT mix (unmodified, control GT third strand). (C) Phase diagram for the 22Py/22GpU mix (propynyl-dU-containing GT third strand). (D) Phase diagram for the 22Py/22GdU mix (dU-containing GT third strand). All experiments were performed in 10 mM sodium cacodylate, 100 mM LiCl, pH 6.9, at variable $MgCl_2$ concentration. Strand concentration: 3 μM. The diagram is divided into 3 areas, labeled "I", "III_{TC}", and "III_{GT}", which correspond to melted strands, pyrimidine (TC) triplex, and GT triplex, respectively. The experimental midpoint of the triplex-to-triplex transition ("3-3" determined at 295 nm) is indicated by filled circles. The experimental position of the GT triplex to single strands (determined at 260 nm) is indicated by open squares.

Table 5: GT Motif vs CT Motif: Triplex-to-Triplex Transition[a]

complex + 22Py	modification	T_m1 295 nm	ΔT_m 295 nm	T_m2 260 nm
22GT	none	19		43
22GTS	PS	24	−1	41
22GTmP	mP	19	+0	42
22GTRNA	RNA	25	+6	39.5
22GTOMe	2′-OMe	25	+6	37.5
22GbU	bromo-U	19	+0	43
22GpU	propynyl-U	17	−2	43.5
22GdU	deoxy-U	8	−11	45.5

[a] T_m1 corresponds to the TC/GT triplex-to-triplex transition determined from analysis of the melting curve recorded at 295 nm. T_m2 corresponds to the GT triplex-to-coil transition determined from analysis of the melting curve recorded at 260 nm. Buffer conditions are 10 mM sodium cacodylate in 0.1 M lithium chloride and 10 mM magnesium chloride at pH 6.9. All T_ms and ΔT_m are given in °C, ±0.5 °C.

transition without any interference from the second transition (melting of the duplex: see Figure 2C, circles).

Figure 6B is a plot of T_m vs magnesium concentration for this system and shows the GT triplex to CT triplex (III to III) phase boundary as well as the GT triplex to coil (III to I) phase boundary. The effect of replacing T with pU and dU is shown in Figures 6C and 6D, respectively. It is clear in Figure 6D that replacing T with dU stabilizes the GT motif and, in doing so, shifts the triplex-to-triplex phase boundary to lower T_m. The CT-to-GT triplex conversion can be monitored at both 295 and 260 nm, and the T_m's are shown in Table 5. The GdU triplex can shift the phase boundary with the CT triplex by 11 °C more than the GT triplex, making GdU the most stable analogue tested, which is in agreement with the results from the simple triplex system.

DISCUSSION

Various chemical modifications of triplex-forming oligonucleotides have been proposed in the past few years. Very little data are available on the relative affinities of such TFOs under identical conditions with the same target. In this study, we have therefore compared different chemical modifications on the three classes of triplexes. This systematic study allowed us to demonstrate that pU and dU offer a significant advantage for triplex formation in the "GT" motif.

Intramolecular vs Intermolecular Triplexes. In most of the experiments described in this paper, the third strand is covalently linked to one strand of the duplex via a CCTT loop. The size of the loop (4 bases) was chosen to allow sufficient flexibility (*33*). Therefore, the triplex-to-duplex transition corresponds to an intramolecular reaction (see Figure 1). The thermodynamic parameters deduced from this type of complex are different from those determined for an intermolecular reaction. This difference mainly concerns the entropic factor, $\Delta S°$, as the covalent link between two interacting strands corresponds to a high local concentration of the third strand and a reduction of the conformational space of the system (*34*).

GT/GA vs Pyrimidine Triplexes. All canonical triplets formed in the Hoogsteen mode (C·G*C+ and T·A*T) or in the reverse-Hoogsteen mode (T·A*T, T·A*A, and T·A*G) are based on the formation of two hydrogen bonds between the base on the third strand and the purine base of the Watson−Crick base pair. In contrast with these shared properties, there are numerous factors that allow one to

Table 6: Effect of TFO Modification on Triplex Stability[a]

name	abbreviation	TC	GT	GA
	Backbone			
phosphorothioate	PS	−	=	=
methylphosphonate	mP	−	=	=
2′-OH	RNA	+	−	≤
2′-OMe	OMe	+	−	≤
	Base			
methylcytosine	mC	+	na	na
uracil	dU	=	+	na
propynyl-U	pU	+	+	na
bromouracil	bU	nd	=	na

[a] Abbreviations: PO, phosphate; PS, phosphorothioate; mP, methylphosphonate; OMe, 2′-*O*-methyl; pU, 5-propynyl-U; bU, 5-bromo-U; dU, 5-deoxyuracil; mC, methyl-C; base modifications are introduced in a regular phosphate DNA backbone; (=) is as stable, (+) more stable, (−) less stable, and (≤) slightly less stable than the parent DNA triplex with a phosphate backbone; na, not applicable (no thymine in the GA motif); nd, not determined.

distinguish between these two classes of triplexes: (i) the isomorphism of some base triplets, (ii) the positive charge on each cytosine in the third strand of a pyrimidine triplex, (iii) the exact location of the third strand in the major groove of DNA, and (iv) the stacking interactions in the third strand.

Effect of Backbone Modifications. Table 6 is a qualitative summary of the effects of base and backbone modifications within the third strand of the TC, GT, and GA triplexes. Backbone modifications have sharply constrasting effects on the three motifs. Phosphorothioate and methylphosphonate substitutions destabilize the TC motif but are accommodated in the GT and GA motifs. This corresponds to the results of Hacia et al. (*35*) obtained by DNase I footprinting. Xodo et al. (*36*) reported a 2 °C drop in the T_m per phosphorothioate substitution in a TC TFO targeted to a hairpin duplex. This destabilization is not due to the formation of a more stable competing structure by the PS TFO as PS and PO TFOs form i-motif tetraplexes with similar T_m (*37*). In the GA motif, the PS substitution has been reported as slightly destabilizing (*38*).

We find that the methylphosphonate substitution significantly destabilizes the TC triplex, in agreement with previous results (*39*). The methylphosphonate TFO in the intermolecular system of Lacroix and Mergny (*40*) did not form a triplex or an i-motif tetraplex. These results are in conflict with the idea that a nonionic substitution should favor triplex formation by overcoming strand repulsion. Interestingly, our results show that the mP substitution favors the GT/GA triplexes, in agreement with the report of Trapane et al. (*41*) which shows that a 2:1 complex of mPdA and POdT or mP(dAG)8 and PO(dTC)8 is more stable than the corresponding PO third strands. Even more intriguing is the fact that a mP oligonucleotide can form a 2:1 complex with a pyrimidine strand of mRNA that can inhibit protein synthesis (*42*). With this result in mind, we are currently investigating the stability of our mP clamp on an RNA pyrimidine strand.

Several articles report that a UC RNA third strand forms a more stable triplex than TC DNA and that GU and GA RNA do not form triplexes. These results are supported by EMSA (*43*), affinity cleavage (*44*), and T_m analyses (*45*, *46*). The TC motif is even further stabilized by 2′-OMe substitution, and our results concur with those obtained by NMR with an intramolecular system (*47*). The solution structure obtained from NMR data revealed that the 2′-OMe third strand imposes the least distortion to the purine strand of the duplex on triplex formation. The sugars of the 2′-OMe and RNA strands also adopted a predominantly C3′-*endo* conformation, which may be more favorable for triplex formation than the C2′-*endo* conformation adopted by a DNA third-strand. Furthermore, the stabilization gained from replacing a DNA phosphate backbone with a 2′-OMe RNA backbone was compounded by replacing C with mC.

Effect of Base Modifications. We chose mC to replace C as a positive control as it is known to significantly stabilize both polynucleotide (*19*) and oligonucleotide TC triplexes (*48*). Replacing T with pU is even more favorable than replacing C with mC, and the stabilization observed is compounded with the double modification of T and C to pU and mC, respectively. The solution structure of an intramolecular system with pU and C in the third strand reveals that increased stacking interaction is gained from the extended π system of pU which stacks favorably with the 5′-nucleotide (*49*).

In the purine motif, the GdU analogue is more stable than either GpU or GbU. The most stable complexes we investigated are a pyrimidine motif DNA triplex composed of pU and mC and a purine motif DNA triplex composed of G and U with T_m's of 44 and 44.5 °C, respectively (10 mM sodium cacodylate, 0.1 M LiCl, 10 mM $MgCl_2$, pH 6.9).

Analysis of the Thermodynamic Parameters. Several conclusions may be drawn from these results: (i) $\Delta H°$ of pyrimidine triplex formation at pH 6.0 varies between −47 and −51 kcal/mol, i.e., -5.4 ± 0.6 kcal/mol of base triplet; (ii) $\Delta H°$ of GT triplex formation is found between −9 and −12 kcal/mol, i.e., -1.2 ± 0.2 kcal/mol per base triplet; (iii) the $\Delta H°$ of purine (GA) triplex formation is very close to 0 (-1 ± 2 kcal/mol, i.e., -0.1 ± 0.2 kcal/mol per base triplet).

In summary, $\Delta H°$ for GT triplex formation is roughly one-third of the value found for the TC triplex, whereas $\Delta H°$ for GA triplex formation is close to 0. This less favorable enthalpy of triplex formation for the GT and GA triplexes is compensated by a more favorable entropic contribution. These results obtained with chemically modified triplexes are in qualitative agreement with our results on DNA triplexes (*6*).

Competition of the Pyrimidine Strand and the Guanine-Rich Strand for Binding to the Core Duplex (The Strand Displacement Phenomenon). Starting from the dissociated strands at 90 °C, upon lowering the temperature, the guanine-rich triplex is formed first without any interference from the pyrimidine hanging strand. At even lower temperatures, the pyrimidine single-strand extension is able to displace the GT strand from the major groove of the duplex. This "triplex-to-triplex" transition is concentration-independent and pH-dependent. This triplex-to-triplex conversion is observed under a large set of experimental conditions and for various chemically modified TFOs. It is the result of the completely different thermodynamic properties for GT and TC triplexes, which allow the relative stabilities of purine and pyrimidine triplexes to be reversed with temperature.

CONCLUSION AND FURTHER DEVELOPMENTS

A previous study allowed a direct comparison of the stabilities of GT, GA, and TC triplexes. We have extended

this work to mixed DNA/RNA/phosphorothioate third strands and base analogues in either strand. In most experiments presented in this paper, experimental conditions were chosen to minimize intra- or intermolecular structures formed by the separated oligonucleotides. It should be pointed out that some modifications may lead to stable undesired folded structures that may hamper triplex formation (*40*). Among the various chemically modified oligonucleotides presented in this study, it is striking to note that deoxyuracil offers a significant advantage over thymine to form a "GT" triplex. This stabilization was confirmed in a different sequence context, with an intermolecular triplex, showing that deoxyuracil should be chosen rather than T in most "GT" TFOs.

The utilization of circular oligonucleotides in the complexes may also strongly influence the choice between the different triplexes. This work was performed with a classical B-DNA duplex, and only the TFO part was chemically modified. It should be interesting to test the substitution of either strand of the DNA Watson−Crick duplex by the corresponding RNA strand in an attempt to mimic an antisense clamp.

ACKNOWLEDGMENT

We thank J. C. François, J. S. Sun, M. Rougée, and C. Hélène for helpful discussions.

REFERENCES

1. Felsenfeld, G., Davies, D. R., and Rich, A. (1957) *J. Am. Chem. Soc. 79*, 2023−2024.
2. Le Doan, T., Perrouault, L., Praseuth, D., Habhoub, N., Decout, J.-L., Thuong, N. T., Lhomme, J., and Hélène, C. (1987) *Nucleic Acids Res. 15*, 7749−7760.
3. Moser, H. E., and Dervan, P. B. (1987) *Science 238*, 645−650.
4. Praseuth, D., Guieysse, A. L., and Hélène, C. (1999) *Biochim. Biophys. Acta 1489*, 181−206.
5. Vasquez, K. M., Narayanan, L., and Glazer, P. M. (2000) *Science 290*, 530−533.
6. Mills, M., Arimondo, P., Lacroix, L., Garestier, T., Hélène, C., Klump, H. H., and Mergny, J. L. (1999) *J. Mol. Biol. 291*, 1035−1054.
7. Sun, J. S., De Bizemont, T., Duval-Valentin, G., Montenay-Garestier, T., and Hélène, C. (1991) *C. R. Acad. Sci., Ser. III 313*, 585−590.
8. Mills, M., and Klump, H. H. (1998) *Nucleosides Nucleotides 17*, 1919−1936.
9. Giovannangeli, C., Montenay-Garestier, T., Thuong, N. T., and Hélène, C. (1992) *Proc. Natl. Acad. Sci. U.S.A. 89*, 8631−8635.
10. Stein, C. A., Mori, K., Loke, S. L., Subasinghe, C., Shinozuka, K., Cohen, J. S., and Neckers, L. M. (1988) *Gene 72*, 333−341.
11. Miller, P. S., McParland, K. B., Jayaraman, K., and Ts'o, P. O. P. (1981) *Biochemistry 20*, 1874−1880.
12. Escudé, C., Sun, J. S., Rougée, M., Garestier, T., and Hélène, C. (1992) *C. R. Acad. Sci., Ser. III 315*, 521−525.
13. Shimizu, M., Konishi, A., Shimada, Y., Inoue, H., and Ohtsuka, E. (1992) *FEBS Lett. 302*, 155−158.
14. Gryaznov, S. M., Lloyd, D. H., Chen, J. K., Schulz, R. G., Dedionisio, L. A., Ratmeyer, L., and Wilson, W. D. (1995) *Proc. Natl. Acad. Sci. U.S.A. 92*, 5798−5802.
15. Summerton, J., and Weller, D. (1997) *Antisense Nucleic Acid Drug Dev. 7*, 187−195.
16. Nielsen, P. E., Egholm, M., Berg, R. H., and Buchardt, O. (1991) *Science 251*, 1497−1500.
17. Plum, G. E. (1998) *Biopolymers 44*, 241−256.
18. Shafer, R. H. (1998) in *Progress in Nucleic Acid Research* (Moldave, K., Ed.) pp 55−94, Academic Press, Inc., New York.
19. Lee, J. S., Woodsworth, M. L., Latimer, L. J. P., and Morgan, A. R. (1984) *Nucleic Acids Res. 12*, 6603−6614.
20. Froehler, B. C., Wadwani, S., Terhorst, T. J., and Gerrard, S. R. (1992) *Tetrahedron Lett. 33*, 5307−5310.
21. Faucon, B., Mergny, J. L., and Hélène, C. (1996) *Nucleic Acids Res. 24*, 3181−3188.
22. Paes, H. M., and Fox, K. R. (1997) *Nucleic Acids Res. 25*, 3269−3274.
23. Roy, C. (1993) *Nucleic Acids Res. 21*, 2845−2852.
24. Scaria, P. V., and Shafer, R. H. (1996) *Biochemistry 35*, 10985−10994.
25. Cantor, C. R., Warshaw, M. M., and Shapiro, H. (1970) *Biopolymers 9*, 1059−1077.
26. Rougée, M., Faucon, B., Mergny, J. L., Barcelo, F., Giovannangeli, C., Garestier, T., and Hélène, C. (1992) *Biochemistry 31*, 9269−9278.
27. Lavelle, L., and Fresco, J. R. (1995) *Nucleic Acids Res. 23*, 2692−2705.
28. Mergny, J. L., Lacroix, L., Han, X., Leroy, J. L., and Hélène, C. (1995) *J. Am. Chem. Soc. 117*, 8887−8898.
29. Manzini, G., Xodo, L. E., Gasparotto, D., Quadrifoglio, F., van der Marel, G. A., and van Boom, J. H. (1990) *J. Mol. Biol. 213*, 833−843.
30. Vo, T., Wang, S. H., and Kool, E. T. (1995) *Nucleic Acids Res. 23*, 2937−2944.
31. Arimondo, P. B., Barcelo, F., Sun, J. S., Maurizot, J. C., Garestier, T., and Hélène, C. (1998) *Biochemistry 37*, 16627−16635.
32. Aich, P., Ritchie, S., Bonham, K., and Lee, J. S. (1998) *Nucleic Acids Res. 26*, 4173−4177.
33. Mills, M., Völker, J., and Klump, H. H. (1996) *Biochemistry 35*, 13338−13344.
34. Völker, J., Osborne, S. E., Glick, G. D., and Breslauer, K. J. (1997) *Biochemistry 36*, 756−767.
35. Hacia, J. G., Wold, B. J., and Dervan, P. B. (1994) *Biochemistry 33*, 5367−5369.
36. Xodo, L., Alunni-Fabbroni, M., Manzini, G., and Quadrifoglio, F. (1994) *Nucleic Acids Res. 22*, 3322−3330.
37. Mergny, J. L., and Lacroix, L. (1998) *Nucleic Acids Res. 26*, 4897−4903.
38. Cogoi, S., Rapozzi, V., Quadrifoglio, F., and Xodo, L. (2001) *Biochemistry 40*, 1135−1143.
39. Miller, P. S., Kipp, S. A., and McGill, C. (1999) *Bioconjugate Chem. 10*, 572−577.
40. Lacroix, L., and Mergny, J. L. (2000) *Arch. Biochem. Biophys. 381*, 153−163.
41. Trapane, T. L., Hogrefe, R. I., Reynolds, M. A., Kan, L. S., and Tso, P. O. P. (1996) *Biochemistry 35*, 5495−5508.
42. Reynolds, M. A., Arnold, L. J., Almazan, M. T., Beck, T. A., Hogrefe, R. I., Metzler, M. D., Stoughton, S. R., Tseng, B. Y., Trapane, T. L., Tso, P. O. P., and Woolf, T. M. (1994) *Proc. Natl. Acad. Sci. U.S.A. 91*, 12433−12437.
43. Semerad, C. L., and Maher, L. J., III (1994) *Nucleic Acids Res. 22*, 5321−5325.
44. Han, H., and Dervan, P. B. (1993) *Proc. Natl. Acad. Sci. U.S.A. 90*, 3806−3810.
45. Roberts, R. W., and Crothers, D. M. (1992) *Science 258*, 1463−1466.
46. Escudé, C., François, J. C., Sun, J. S., Ott, G., Sprinzl, M., Garestier, T., and Hélène, C. (1993) *Nucleic Acids Res. 21*, 5547−5553.
47. Asensio, J. L., Carr, R., Brown, T., and Lane, A. N. (1999) *J. Am. Chem. Soc. 121*, 11063−11070.
48. Xodo, L. E., Manzini, G., Quadrifoglio, F., van der Marel, G. A., and van Boom, J. H. (1991) *Nucleic Acids Res. 19*, 5625−5631.
49. Phipps, A. K., Tarkoy, M., Schultze, P., and Feigon, J. (1998) *Biochemistry 37*, 5820−5830.

BI011122M